Scientia Iranica A (2014) 21(1), 1–10

Sharif University of Technology
Scientia Iranica
Transactions A: Civil Engineering
www.scientiairanica.com

A node enrichment strategy in collocated discrete least squares meshless method for the solution of generalized Newtonian fluid flow

M. Lashckarbolok[a], E. Jabbari[a,*] and K. Vuik[b]

a. *School of Civil Engineering, Iran University of Science and Technology, Tehran, 16846, Iran.*
b. *Delft Institute of Applied Mathematics, 2628 CD Delft, Mekelweg 4, room HB 03.070, Netherlands.*

Received 4 July 2012; received in revised form 11 May 2013; accepted 22 July 2013

KEYWORDS
Node enrichment;
Meshless methods;
Carreau-Yasuda fluid;
Least squares technique.

Abstract. A simple node enrichment strategy using a gradient based error estimator is presented for the Collocated Discrete Least Squares (CDLS) meshless method. Also, a procedure is defined to distribute collocation points according to the field nodes position. Here, shape functions are constructed using the Radial Point Interpolation Method (RPIM). As temporal discretization, a first-order accurate scheme, named the semi-incremental fractional step method, is used. One of the advantages of this scheme is its capability of using large time step sizes for the solution of governing equations on steady state problems. The capability of the presented strategy is shown by investigating the Carreau-Yasuda fluid flow model in solving lid-driven cavity flow problems with different curve fitting indices values.

1. Introduction

There are numerous studies about the numerical simulation of non-Newtonian fluid flow (see [1]). Most of these investigations are performed in a finite element and finite volume field. Using a mesh or grid is a basic characteristic of these conventional numerical methods for the solution of governing equations. During recent years, significant efforts have been devoted to the development of so-called meshless or meshfree methods. The purpose of this methodology is to get rid of the structure of the mesh and to approximate the solution using scattered nodes inside and on the boundaries of the domain. A detailed review on meshless methods is provided by Belytschko [2], Liu [3] and Liu and Gu [4]. Each efficient numerical method should possess some properties, such as a strong mathematical basis, simplicity and parameter independency. The CDLS method is a truly meshless method based on a simple least squares principle. Initially, Arzani and Afshar [5] developed the Discrete Least Squares (DLS) meshless method for the solution of Poisson equations. The main idea was adopted from the least squares technique in FEM. Subsequently, Afshar and Lashckarbolok [6] used collocation points in the DLS method and developed the CDLS meshless method. According to their research, collocation points have significant effects on the performance of the method. Recent research into the CDLS method can be found in [7-10].

It is desirable to refine the spatial domain where the numerical errors are high. However, sometimes there is not a priori knowledge about the distribution of the numerical errors. Adaptive refinement strategies based on error estimators are useful tools to improve the efficiency of the numerical methods by refining the computational domain where it is needed [11]. These

*. *Corresponding author. Tel.: +98 21 77240398*
E-mail addresses: mlbolok@iust.ac.ir (Mohsen Lashckarbolok), jabbari@iust.ac.ir (Ebrahim Jabbari), c.vuik@tudelft.nl (Kees Vuik)

methods have been extensively used by finite element practitioners to solve various engineering problems [12]. Several error estimates and adaptive refinement methods have also been proposed for meshless methods. An adaptive refinement strategy, based on a node-moving methodology, was developed in conjunction with the collocated method for one-dimensional hyperbolic problems by Afshar and Lashckarbolok [6]. The method was extended by Firoozjaee and Afshar [13] for the adaptive solution of hyperbolic problems in two dimensions. The adaptive refinement technique based on the node-moving strategy is extended for the adaptive solution of incompressible Navier-Stokes equations [11]. In that node-moving strategy, the value of a least squares functional of the residual of the governing differential equation at nodal points (or field nodes) is considered a measure of the error and is used to estimate the distribution of the numerical error. The node-moving technique is then employed to relocate the field nodes such that more nodes are used to represent areas of the problem domain with large errors. The problem is then resolved on the refined distribution of nodes for higher accuracy. In this study, a simple node enrichment process, along with a gradient based error estimator, is presented for the CDLS method in the context of generalized Newtonian fluid flow. Errors are estimated by considering both velocity and viscosity gradients. Since, for more field nodes, more collocation points are needed to calculate residuals more accurately, a strategy is presented to allocate collocation points according to the field nodes positions. As temporal discretization, a fractional step method is used. The fractional step method performs the advance in time in three main steps: First, the momentum equation is used to calculate an intermediate velocity and then, in the second step, the pressure is evaluated using the intermediate velocity. Finally, in the third step, the velocity can be calculated using the intermediate velocity and pressure. Several fractional step methods have been introduced in the literature. The non-incremental fractional step method proposed by Chorin [14] is one of the most popular fractional step methods. Another well-known method, the incremental fractional step method, was proposed by modifying the method of Chorin through adding the previous value of the pressure gradient to the momentum equation [15]. The incremental fractional step method and its variants need to satisfy the LBB (inf-sup) condition to lead to a stable solution [16]. On the contrary, the non-incremental fractional step method and its variants are not required to satisfy the LBB condition [16]. Despite this advantage, unfortunately, they yield inaccurate solutions when large time step sizes are used [17]. Dealing with steady-state problems, it is favourable to use large time step sizes to reduce the computational effort. Recently, Firoozjaee and Afshar [9] presented a new fractional step method, named the semi-incremental fractional step method, to use the advantages of the incremental fractional step method without suffering from LBB condition satisfaction. In this study, the proposed method in [9] is used for temporal discretization of generalized Newtonian fluid equations.

2. CDLS meshless method

The CDLS meshless method formulation was given in [6] and [13]. Here, this formulation is given again in more detail. Consider the general form of a partial differential equation:

$$\Im(u) = f \qquad \text{in} \quad \Omega, \tag{1}$$

$$\Re(u) = g \qquad \text{on} \quad \Gamma_t, \tag{2}$$

$$u = \bar{u} \qquad \text{on} \quad \Gamma_u. \tag{3}$$

Here, u denotes the unknown function. $\Im$ and $\Re$ are some proper differential operators defined on the problem domain, Ω, and its Neumann boundary, Γ_t, respectively. Γ_u represents the Dirichlet boundary with a prescribed value of $\bar{u}$, and f is the source term in the problem domain. The philosophy of the least squares method is to find an approximate solution that minimizes the least squares functional to be defined later. As shown in Figure 1, the problem domain and its boundaries are discretized by field nodes and collocation points. Assume n_p is the number of nodes in the domain and on the boundaries. Besides field nodes, collocation points are used in the problem domain and on its boundaries. In this methodology, in each field node, one collocation point has to be placed, as shown in Figure 1. The approximated value of function u at collocation point k, with coordinate x_k, can be obtained through the following interpolation:

$$u(x_k) = \sum_{i=1}^{\bar{n}_k} N_i(x_k).u_i, \tag{4}$$

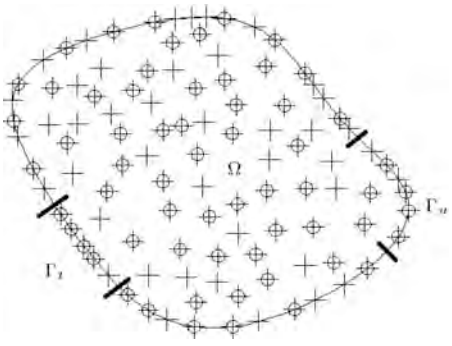

Figure 1. The domain discretized by field nodes (circles) and collocation points (cross signs).

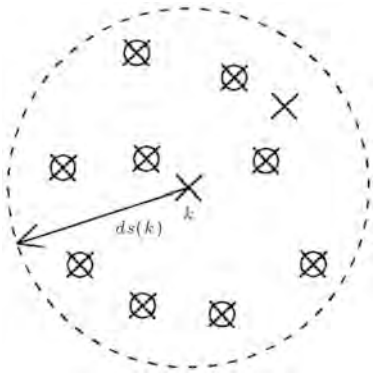

Figure 2. Compact support of the kth collocation.

where u_i is the value of the unknown function at the ith field node. $\overline{n}_k$ is the number of field nodes that the kth collocation point, with coordinate x_k, has in its domain. This idea of compact support is shown in Figure 2. To set up such a domain for each collocation point, radius ds is defined so that a specific number of field nodes are placed into its support domain. In Eq. (4), $N_i(x_k)$ is the value of the shape function of the ith node at the kth collocation point, which will be defined later. In this paper, first, the number of nodes to support the collocation points is defined as $\overline{n}_k$. Then, for each collocation, a radius (ds) is determined so that $\overline{n}_k$ nodes are placed in the domain of that collocation. Substitution of Eq. (4) into Eqs. (1)-(3) leads to the differential equation residual (R^d), the Neumann boundary condition residual (R^t) and the Dirichlet boundary condition residual (R^u) defined as follows, respectively:

$$R_k^{(d)} = \Im(u(x_k)) - f(x_k)$$
$$= \sum_{i=1}^{\bar{n}_k} \Im(N_i(x_k))u_i - f(x_k) \qquad (k = 1 \sim M), \quad (5)$$

$$R_k^{(t)} = \Re(u(x_k)) - g(x_k)$$
$$= \sum_{i=1}^{\bar{n}_k} \Re(N_i(x_k))u_i - g(x_k) \qquad (k = 1 \sim n_t), \quad (6)$$

$$R_k^{(u)} = u(x_k) - \bar{u} = \sum_{i=1}^{\bar{n}_k} (N_i(x_k))u_i - \bar{u}$$
$$(k = 1 \sim n_u). \quad (7)$$

In these relations, n_t and n_u are the number of collocation points located on the field nodes in the Neumann and Dirichlet boundaries, respectively. M is the total number of collocation points. Now, the following least squares functional of all residuals at all collocation points can be constructed as:

$$J = \frac{1}{2}\left(\sum_{k=1}^{M}\left[R_k^{(d)}\right]^2 + \alpha.\sum_{k=1}^{n_t}\left[R_k^{(t)}\right]^2 + \beta.\sum_{k=1}^{n_u}\left[R_k^{(u)}\right]^2\right). \quad (8)$$

Parameters α and β in this equation represent the relative weight of the boundary residuals, with respect to the interior residuals, named penalty coefficients.

Minimization of Eq. (8), with respect to parameters u_i leads to the following system of linear equations:

$$\mathbf{KU} = \mathbf{F}, \quad (9)$$

in which $\mathbf{U}$ is the vector of parameters in field nodes. The typical components of matrix $\mathbf{K}$ and the right hand side vector, $\mathbf{F}$, are defined as:

$$K_{ij} = \sum_{k=1}^{M} \Im(N_i(x_k)).\Im(N_j(x_k))$$
$$+ \alpha \sum_{k=1}^{n_t} \Re(N_i(x_k)).\Re(N_j(x_k))$$
$$+ \beta \sum_{k=1}^{n_u} N_i(x_k).N_j(x_k) \qquad i, j = 1, \cdot, n_p, \quad (10)$$

$$F_i = \sum_{k=1}^{M} \Im(N_i(x_k))f(x_k) + \alpha \sum_{k=1}^{n_t} \Re(N_i(x_k))g(x_k)$$
$$+ \beta \sum_{k=1}^{n_u} N_i(x_k).\bar{u} \qquad i = 1, \cdots, n_p. \quad (11)$$

The stiffness matrix, $\mathbf{K}$, in Eq. (9) is symmetric, even for non-self-adjoint operators. The size of $\mathbf{K}$ just depends on the number of field nodes (n_p), and the number of collocation points (M) does not increase the size of the final system of equations. It is also sparse since a small number of nodes contribute to the function evaluation for a collocation point. Therefore, the final system of equations can be solved by effective iterative solvers.

3. Governing equations

Governing equations are comprised of continuity, momentum and constitutive equations for the two dimensional incompressible flow of a generalized Newtonian fluid. They are in Cartesian coordinates given by:

$$\frac{\partial u^*}{\partial t^*} + u^*\frac{\partial u^*}{\partial x^*} + v^*\frac{\partial u^*}{\partial y^*} = -\frac{1}{\rho^*}\frac{\partial P^*}{\partial x^*}$$
$$+ \frac{1}{\rho^*}\left(\frac{\partial \tau_{xx}^*}{\partial x^*} + \frac{\partial \tau_{xy}^*}{\partial y^*}\right), \quad (12)$$

$$\frac{\partial v^*}{\partial t^*} + u^*\frac{\partial v^*}{\partial x^*} + v^*\frac{\partial v^*}{\partial y^*} = -\frac{1}{\rho^*}\frac{\partial P^*}{\partial y^*} + \frac{1}{\rho^*}\left(\frac{\partial \tau^*_{yx}}{\partial x^*} + \frac{\partial \tau^*_{yy}}{\partial y^*}\right), \quad (13)$$

$$\frac{\partial u^*}{\partial x^*} + \frac{\partial v^*}{\partial y^*} = 0, \quad (14)$$

$$\tau^*_{xx} = 2\eta^*\frac{\partial u^*}{\partial x^*}, \quad (15)$$

$$\tau^*_{xy} = \tau^*_{yx} = \eta^*\left(\frac{\partial u^*}{\partial y^*} + \frac{\partial v^*}{\partial x^*}\right), \quad (16)$$

$$\tau^*_{yy} = 2\eta^*\frac{\partial v^*}{\partial y^*}, \quad (17)$$

where u^*, v^* and P^* are the velocity component in the x direction, the velocity component in the y direction and the pressure, respectively. η^* is the generalized Newtonian viscosity, which depends on the local shear rate (under isothermal conditions). In Newtonian fluid, η^* is constant for the entire flow field. In this study, the Carreau-Yasuda model is used to describe the fluid viscosity behaviour. It is given by the following formula:

$$\eta^* = \eta^*_\infty + (\eta^*_0 - \eta^*_\infty)\left[1 + (\lambda^*)^a.\dot{\gamma}^{*\frac{a}{2}}\right]^{\frac{n-1}{a}}, \quad (18)$$

where $\dot{\gamma}^*$, λ^*, n, η^*_∞, η^*_0 and a are the second invariant of the rate of the deformation tensor, characteristic time, power index, infinite shear rate viscosity, zero shear rate viscosity and a dimensionless parameter, respectively. $\dot{\gamma}^*$ in the Cartesian coordinate is defined by:

$$\dot{\gamma}^* = 2\left(\frac{\partial u^*}{\partial x^*}\right)^2 + 2\left(\frac{\partial v^*}{\partial y^*}\right)^2 + \left(\frac{\partial u^*}{\partial y^*} + \frac{\partial v^*}{\partial x^*}\right)^2. \quad (19)$$

The above equations can be non-dimensionalized through selection of appropriate scales, as follows:

$$t = \frac{t^*U_0}{L}, \qquad x = \frac{x^*}{L},$$

$$y = \frac{y^*}{L}, \qquad u = \frac{u^*}{U_0},$$

$$P = \frac{P^*}{\rho_0 U_0^2}, \qquad \rho = \frac{\rho^*}{\rho_0},$$

$$\mathrm{Cu} = \frac{\lambda^* U_0}{l_0}, \qquad \eta = \frac{\eta^*}{\eta^*_0},$$

where U_0, l_0, λ_0 and Cu are the reference values of density, velocity, length, characteristic time and Carreau number, respectively. Using constitutive equations, Eqs. (12)-(13) in dimensionless form are given by:

$$\frac{\partial u}{\partial t} + u\frac{\partial u}{\partial x} + v\frac{\partial u}{\partial y} = -\frac{\partial P}{\partial x} + \frac{1}{\mathrm{Re}}\left[2\frac{\partial \eta}{\partial x}.\frac{\partial u}{\partial x} + \frac{\partial \eta}{\partial y}\left(\frac{\partial u}{\partial y} + \frac{\partial v}{\partial x}\right) + \eta\left(\frac{\partial^2 u}{\partial y^2} + \frac{\partial^2 u}{\partial x^2}\right)\right], \quad (20)$$

$$\frac{\partial v}{\partial t} + u\frac{\partial v}{\partial x} + v\frac{\partial v}{\partial y} = -\frac{\partial P}{\partial y} + \frac{1}{\mathrm{Re}}\left[2\frac{\partial \eta}{\partial y}.\frac{\partial v}{\partial y} + \frac{\partial \eta}{\partial x}\left(\frac{\partial u}{\partial y} + \frac{\partial v}{\partial x}\right) + \eta\left(\frac{\partial^2 v}{\partial y^2} + \frac{\partial^2 v}{\partial x^2}\right)\right], \quad (21)$$

where:

$$\mathrm{Re} = \frac{\rho_0 U_0 l_0}{\eta^*_0}. \quad (22)$$

Re and ρ_0 are Reynolds number and reference density, respectively. The above equations are analogous to the following vectorized equation:

$$\frac{\partial \mathbf{U}}{\partial t} + u.\frac{\partial \mathbf{U}}{\partial x} + v.\frac{\partial \mathbf{U}}{\partial y} = -\nabla P + \frac{1}{\mathrm{Re}}\left(\mathbf{A}\frac{\partial \mathbf{U}}{\partial x} + \mathbf{B}\frac{\partial \mathbf{U}}{\partial y} + \mathbf{C}\frac{\partial^2 \mathbf{U}}{\partial x^2} + \mathbf{D}\frac{\partial^2 \mathbf{U}}{\partial y^2}\right) + E, \quad (23)$$

where:

$$\mathbf{U} = \begin{bmatrix} u \\ v \end{bmatrix}, \qquad \mathbf{A} = \begin{bmatrix} 2\frac{\partial \eta}{\partial x} & 0 \\ 0 & \frac{\partial \eta}{\partial x} \end{bmatrix},$$

$$\mathbf{B} = \begin{bmatrix} \frac{\partial \eta}{\partial y} & 0 \\ 0 & 2\frac{\partial \eta}{\partial y} \end{bmatrix}, \qquad \mathbf{C} = \begin{bmatrix} \eta & 0 \\ 0 & \eta \end{bmatrix},$$

$$\mathbf{D} = \begin{bmatrix} \eta & 0 \\ 0 & \eta \end{bmatrix}, \qquad E = \begin{bmatrix} \frac{\partial \eta}{\partial y}.\frac{\partial v}{\partial x} \\ \\ \frac{\partial \eta}{\partial x}.\frac{\partial u}{\partial y} \end{bmatrix}.$$

4. Temporal discretization

Temporal discretization of the equations in their primitive form is performed by the fractional step method. Fractional step methods perform the advance in time in three main steps; first, the momentum equation is used to obtain the intermediate velocity, $\mathbf{U}'$. Then, in the next step, the pressure is evaluated using the intermediate velocity. Finally, in the third step, the velocity is calculated using the intermediate velocity

and the pressure. In this method, the split form of the momentum equation is written as follows:

$$\frac{\mathbf{U}' - \mathbf{U}^{\lambda}}{\Delta t} + u^{\lambda}.\frac{\partial \mathbf{U}'}{\partial x} + v^{\lambda}.\frac{\partial \mathbf{U}'}{\partial y} = \frac{1}{\mathrm{Re}}\left(\mathbf{A}^{\lambda}\frac{\partial \mathbf{U}'}{\partial x} + \mathbf{B}^{\lambda}\frac{\partial \mathbf{U}'}{\partial y} + \mathbf{C}^{\lambda}\frac{\partial^2 \mathbf{U}'}{\partial x^2} + \mathbf{D}^{\lambda}\frac{\partial^2 \mathbf{U}'}{\partial y^2}\right) + E^{\lambda} - \theta.\nabla P^{\lambda}. \quad (24)$$

$\mathbf{U}'$ and $\mathbf{U}^{\lambda}$ are velocities at the intermediate and previous time step, respectively. θ is a parameter with a value between 0 and 1; $\theta = 1$ makes the method incremental and $\theta = 0$ makes it non-incremental. In this paper, θ is always chosen to equal 0.5. After calculating the intermediate velocities ($\mathbf{U}'$), the pressure field can be obtained using the Poisson equation for pressure.

$$\frac{\partial^2 P^{\lambda+1}}{\partial x^2} + \frac{\partial^2 P^{\lambda+1}}{\partial y^2} = \frac{1}{\Delta t}\left(\frac{\partial u'}{\partial x} + \frac{\partial v'}{\partial y}\right) + \theta.\left(\frac{\partial^2 P^{\lambda}}{\partial x^2} + \frac{\partial^2 P^{\lambda}}{\partial y^2}\right). \quad (25)$$

For Eq. (25), operators L and f in Eqs. (10) and (11) can be written as:

$$L(.) = \frac{\partial^2(.)}{\partial x^2} + \frac{\partial^2(.)}{\partial y^2}, \quad (26)$$

$$f = \frac{1}{\Delta t}\left(\frac{\partial u'}{\partial x} + \frac{\partial v'}{\partial y}\right) + \theta.\left(\frac{\partial^2 P^{\lambda}}{\partial x^2} + \frac{\partial^2 P^{\lambda}}{\partial y^2}\right). \quad (27)$$

Using these pressure values, the velocity field can be updated as follows:

$$u^{\lambda+1} = u' - \Delta t\left(\frac{\partial P^{\lambda+1}}{\partial x} - \theta\frac{\partial P^{\lambda}}{\partial x}\right), \quad (28)$$

$$v^{\lambda+1} = v' - \Delta t\left(\frac{\partial P^{\lambda+1}}{\partial y} - \theta\frac{\partial P^{\lambda}}{\partial y}\right). \quad (29)$$

5. Collocation generation

Collocation points have significant effects on the accuracy and even on the convergence of the method [6]. However, there is not a well defined procedure to distribute these points. It is clear that parts of the problem domain with denser field nodes require denser collocation points. In the present study, Delaunay triangles are used to specify the position of collocation points. First, all the field nodes are connected to each other by Delaunay triangles. Then, collocation points are determined to be in the middle of each triangle side. As mentioned before, on each field node, a collocation point also has to be placed. This simple strategy guarantees that there are enough collocation points everywhere according to field node positions. In Figure 3, the position of the collocation points in part of a sample domain, with respect to field nodes, is shown.

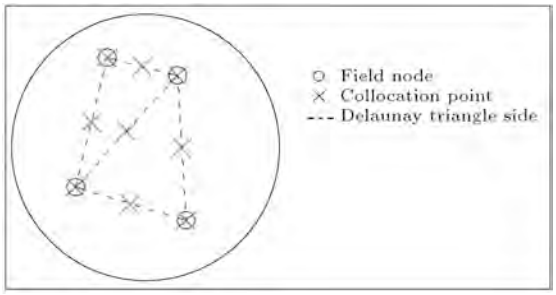

Figure 3. Collocation points position in a sample domain.

6. Error estimate and node enrichment strategy

A gradient based error estimator is used here. It is based on summation of the normalized velocities and viscosity gradients. It is given by:

$$\text{Error} = \frac{\left|\frac{\partial u}{\partial x}\right|}{a} + \frac{\left|\frac{\partial u}{\partial y}\right|}{b} + \frac{\left|\frac{\partial v}{\partial x}\right|}{c} + \frac{\left|\frac{\partial v}{\partial y}\right|}{d} + \frac{\left|\frac{\partial \eta}{\partial x}\right|}{e} + \frac{\left|\frac{\partial \eta}{\partial y}\right|}{f},$$

where a, b, c, d, e and f are the maximum value of $\left|\frac{\partial u}{\partial x}\right|$, $\left|\frac{\partial u}{\partial y}\right|$, $\left|\frac{\partial v}{\partial x}\right|$, $\left|\frac{\partial v}{\partial y}\right|$, $\left|\frac{\partial \eta}{\partial x}\right|$ and $\left|\frac{\partial \eta}{\partial y}\right|$, respectively. To enrich field nodes, in the first step, the estimated errors are evaluated at all collocation points. Then, a finite amount of collocation points with high errors are chosen by sorting the errors. Finally, these chosen collocations turn into field nodes for another solution procedure. To start another solution procedure, again, new collocation points must be generated, according to the new distribution of nodes, as described earlier.

7. Shape function construction

In this study, RPIM is used to construct shape functions. Detailed description of the procedure is available elsewhere [2,3]. In the following numerical examples, a multi quadratic radial basis function augmented with polynomials of completed second order is used in the radial point interpolation method. The multi quadratic radial basis function (q) used in this paper is given by:

$$q(r) = (ds^2 + r^2)^{2.03}, \quad (30)$$

where ds is the radius of the compact support domain defined earlier. In the following numerical examples,

ds is always chosen for each collocation point, so that 25 nodes are placed into the support domain of that collocation.

8. Numerical examples

In this study, Carreau-Yasuda fluid flow in a square cavity is solved by a semi-incremental scheme in temporal discretization and a node enrichment process in spatial discretization. In temporal discretization, the semi incremental factor, θ, is taken as 0.5 in all problems. For the sake of simplicity, η_0^* and η_∞^* are chosen to be one and zero, respectively. Eq. (18) shows that for a very low value of the characteristic time (or Carreau number), the fluid behaves like a Newtonian fluid. In this case, viscosity is independent of n and a. For a very high value of Carreau number, in Eq. (18), constant 1 can be neglected considering the typical values of $\mathrm{Cu}^a\dot{\gamma}^{0.5a}$ and, hence, the fluid behaves like a power law fluid. The problem is solved by different curve fitting parameters. Three cases are considered, which are listed in Table 1. Each case is solved in two steps. First, the problem is solved using a uniform distribution of nodes. Then, according to estimated errors, some nodes are added to the previous nodes and the problem is solved again. Comparison is performed whenever well known published data is available. In all of the following examples, time step size is chosen to equal 0.01. Regarding penalty coefficients, they should be large enough to ensure boundary condition satisfaction. In this study, penalty coefficients are chosen to be $\alpha = \beta = 10^7$ for all cases. The lid-driven cavity flow problem is characterized by a square cavity in which the driving force for the flow is the shear created by a moving lid. The geometry and boundary condition of this problem are shown in Figure 4. Case (I) is equal to a power-law fluid flow with Re = 100 and index $n = 0.5$. In this case, Bell and Surana results [18] are used for comparison. To show the benefit of the enrichment procedure, the problem is first solved using 145 uniform nodes. Then, it is solved again by adding 144 extra nodes in two ways. First, these extra nodes are distributed among the previous nodes uniformly. Second, the extra nodes are distributed among the previous nodes using the enrichment procedure. These two domain discretizations are shown in Figure 5. It should be noted that for the following figures, collocation points located on field nodes are not shown. To make a comparison, the horizontal velocity component profile at the mid-span of the cavity is shown in Figure 6. It shows that with the same number of nodes, the enriched field node distribution shows a much better accuracy than uniform field node distribution. In the next example, case (I) is solved more accurately by distribution of 545 nodes. Using the defined procedure, collocation points are made. Nodes and collocation points are shown in Figure 7. The computed stream functions, before enrichment, are shown in Figure 8. Then, errors are estimated and using the enrichment procedure, 500 new field nodes are added. The new distribution of field nodes is shown in Figure 9, and the computed stream functions using enriched nodal distribution are shown in Figure 10. Case (II) is equal to a power-law fluid flow with Re = 100 and $n = 1.5$. In this case, Bell and Surana results [18] are also used for comparison. The procedure is the same as for case (I). Enriched field node distribution and collocation points are shown in Figure 11. To show the adjustment of the added nodes, counters for estimated errors are shown in Figure 12. In Figure 13, the stream function contours are depicted for this case. Case (III) is equal to a Newtonian fluid at Re=100. This case is compared with the results of Ghia and Shin [19] and the enriched field nodes and computed stream lines are shown in Figures 14 and 15. In Figures 16 and 17, the velocity profiles computed after the enrichment procedure are compared with the results of [18,19]. To show the effect of this nodal enrichment on the convergence of the method, in Figures 18 and 19, the convergence curves are shown for cases (I) and

Table 1. Problems parameters.

Case number	Cu	n	a	Re
(I)	10	0.5	2	31.6228
(II)	10	1.5	2	316.228
(III)	0.01	1.5	2	100

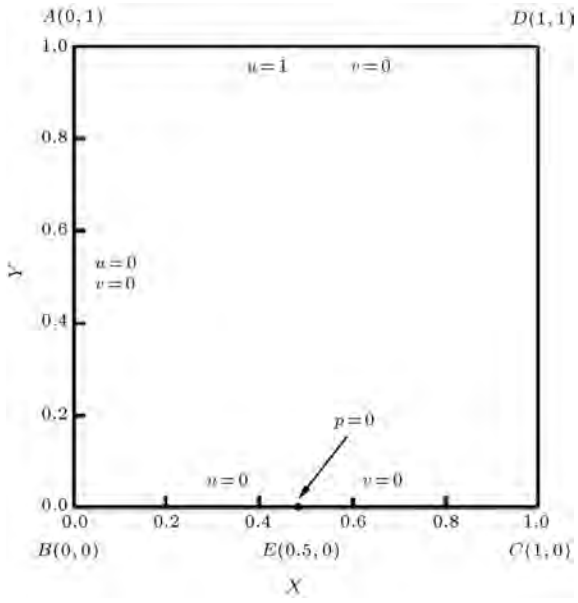

Figure 4. Boundary condition in lid-driven cavity flow problem [8].

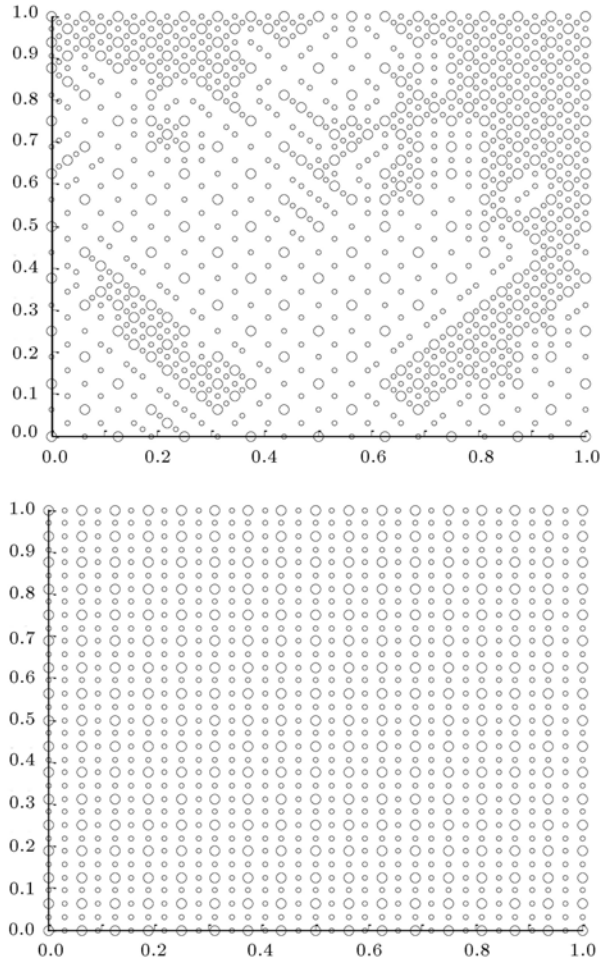

Figure 5. Domain discretization enrichment strategy (up) and uniform distribution (down); bigger circles are field nodes and smaller are collocation points.

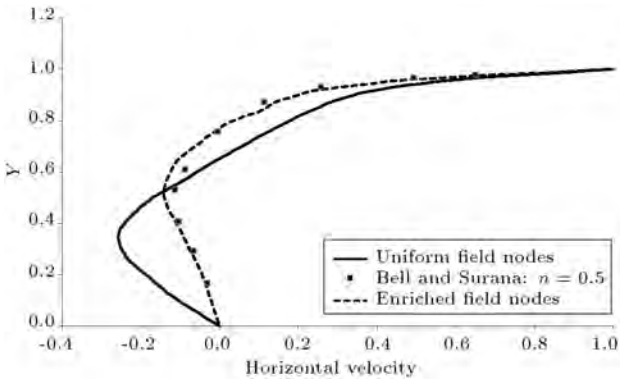

Figure 6. Case (I) - u profile along vertical centre line (comparison between enriched and uniform field node distribution that were shown in Figure 5).

(II). According to those figures, the problem converges sooner after enrichment. The convergence index is defined as below:

$$CI = Log\left(\frac{\max(u^{\lambda+1} - u^{\lambda})}{M}\right). \quad (31)$$

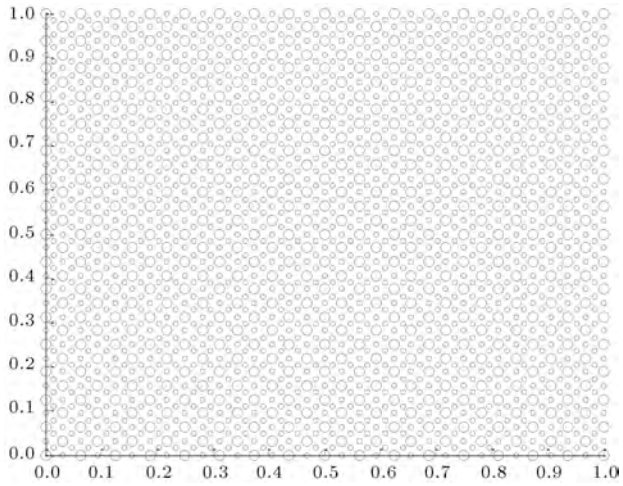

Figure 7. Uniform distribution of nodes (bigger circles) and generated collocation points (smaller circles) include 545 nodes and 2113 collocation points.

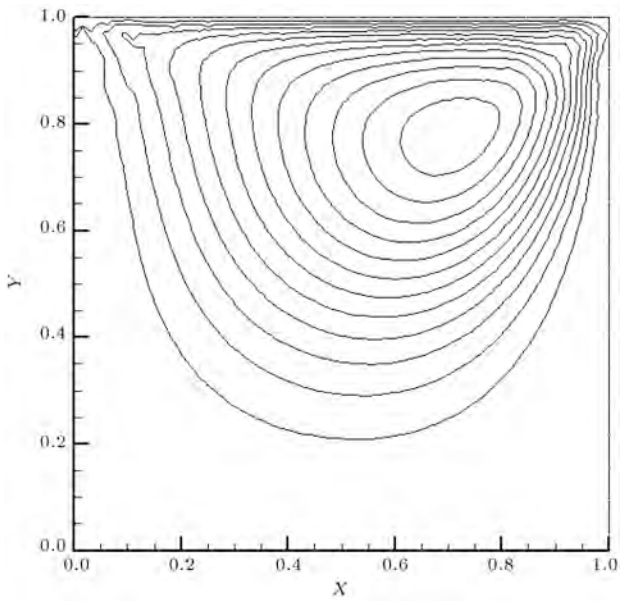

Figure 8. Case (I) - Stream function counters for case (I) using uniform nodal distribution that was shown in Figure 7.

9. Conclusions

In this paper, a node enrichment strategy, along with a gradient based error estimator, was presented for the collocated discrete least squares meshless method. The estimator considers both viscous and inertia gradients. It can be found from the numerical examples that for high Reynolds numbers, the enriched nodes focus on the positions where high velocity gradients are expected (cases (II) and (III)). With low Reynolds numbers or more viscose fluids, the new nodes are concentrated on areas with a higher gradient of viscosity (case (I)). Since the new field node distribution also needs a new collocation distribution, a simple

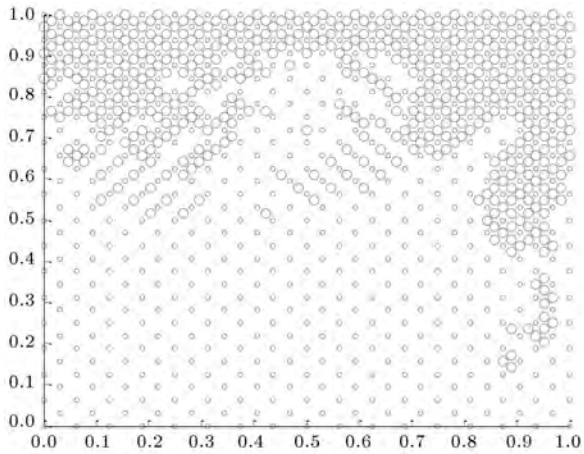

Figure 9. New added nodes (bigger circles) beside old nodes (smaller circles) make new domain discretization.

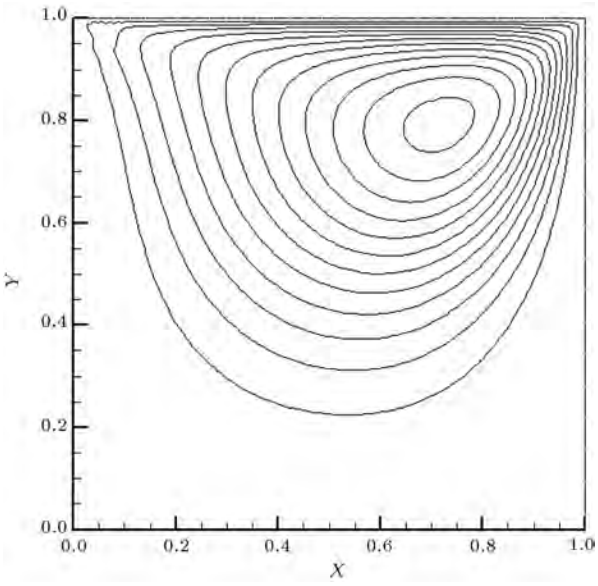

Figure 10. Case (I) - Stream function counters using enriched nodal distribution that was shown in Figure 9.

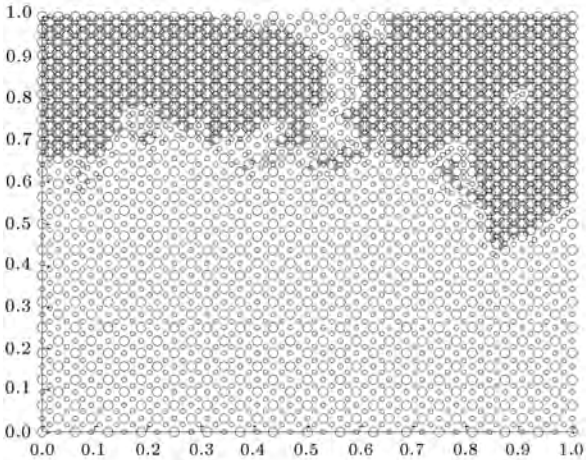

Figure 11. Case (II) - Enriched nodes (bigger circles) and generated collocation points (smaller circles).

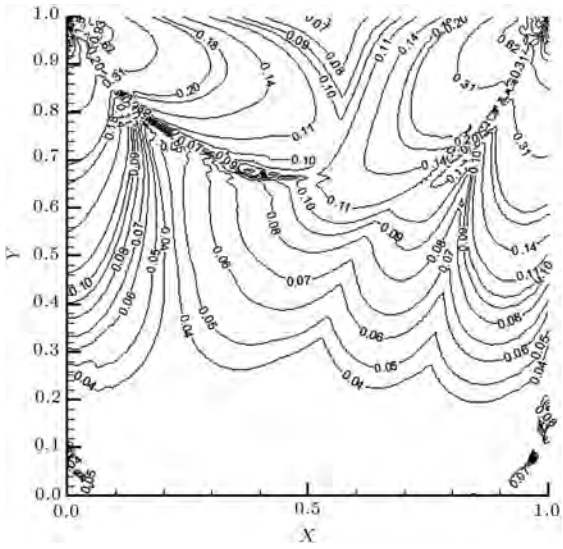

Figure 12. Case (II) - Estimated errors counters in logarithmic scale.

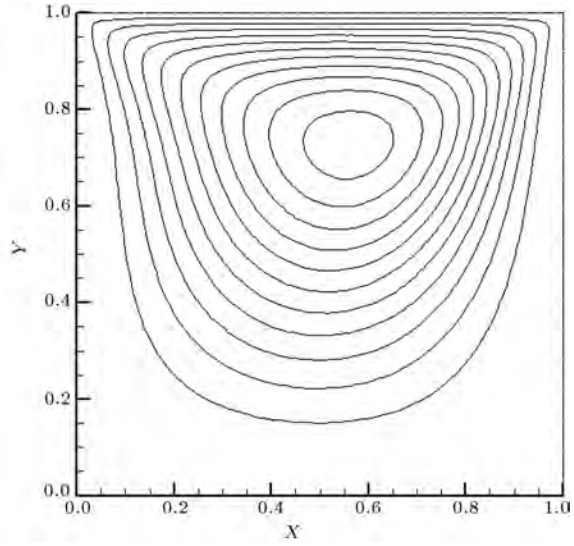

Figure 13. Case (II) - Stream function counters using enriched nodal distribution that was shown in Figure 11.

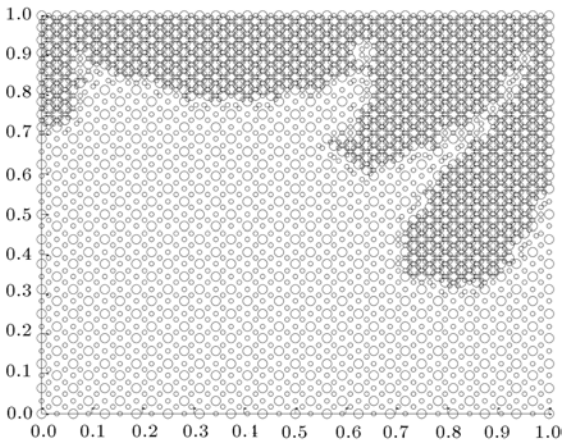

Figure 14. Case (III) - Enriched nodes (bigger circles) and generated collocation points (smaller circles).

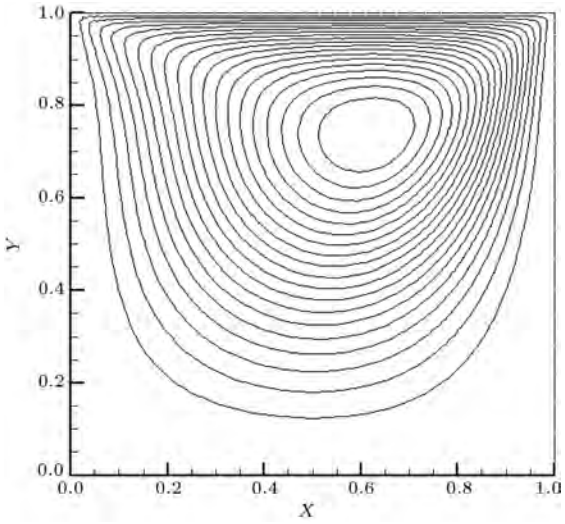

Figure 15. Case (III) - Stream function counters using enriched nodal distribution that was shown in Figure 14.

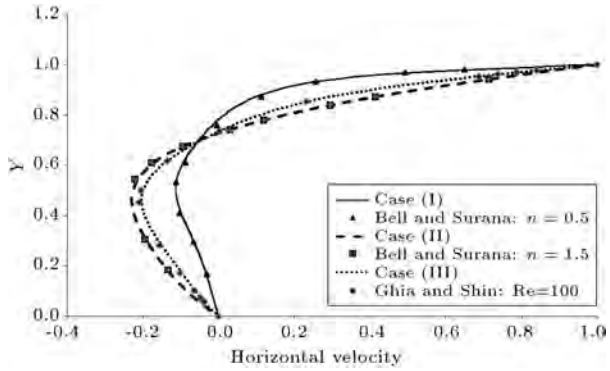

Figure 16. u profile along vertical centre line after node enrichment.

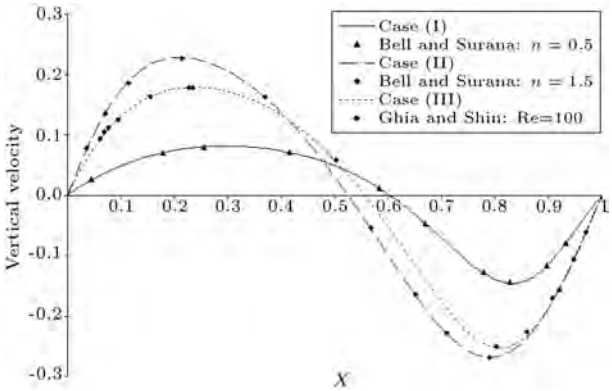

Figure 17. v profile along horizontal centre line after node enrichment.

procedure was defined to distribute collocation points according to field node positions. As temporal discretization, a first-order accurate scheme, named the semi-incremental fractional step method, was used to guarantee the stability and accuracy of the method, regardless of field node distribution. The scheme was

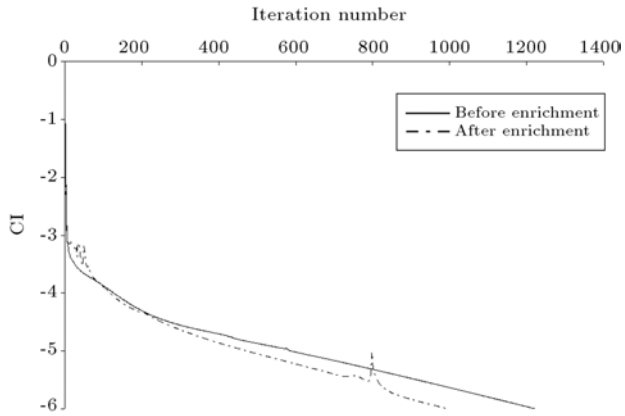

Figure 18. Convergence curves for case (I).

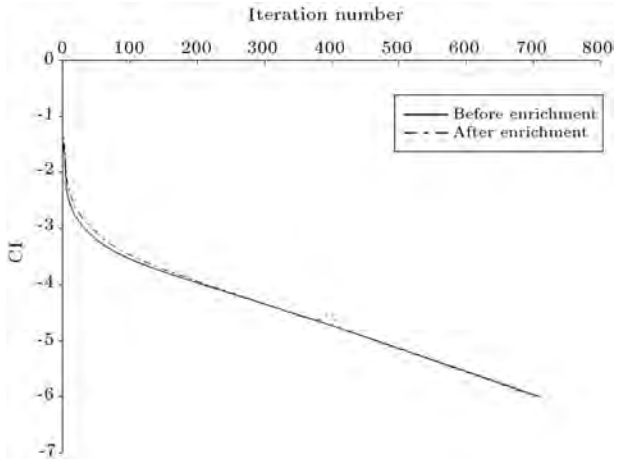

Figure 19. Convergence curves for case (II).

used to solve the lid-driven cavity flow of a Carreau-Yasuda fluid in different curve fitting indices values. The computed solutions show good agreement with the solutions reported in the literature.

References

1. Owens, R.G. and Timothy, N.P., *Computational Rheology*, Imperial College Press, London, UK (2002).
2. Belytschko, T. "Meshless methods: An overview and recent developments", *Computer Methods in Applied Mechanics and Engineering*, **139**(1-4), pp. 3-47 (1996).
3. Liu, G.R., *Mesh Free Methods: Moving Beyond the Finite Element Method*, **1**, 1st Ed., CRC Press, Boca Raton, USA (2002).
4. Liu, G.R. and Gu, Y.T., *An Introduction to Meshless Methods and Their Programming*, 1st Ed., Springer, Berlin, Germany (2005).
5. Arzani, H. and Afshar, M.H. "Solving Poisson's equations by the discrete least squares meshless method", *Boundary Elements and Other Mesh Reduction Methods XXVIII*. WIT Press, Skiathos, Greece, pp. 23-32 (2006).

6. Afshar, M.H. and Lashckarbolok, M. "Collocated discrete least-squares (CDLS) meshless method: Error estimate and adaptive refinement", *International Journal for Numerical Methods in Fluids*, **56**(10), pp. 1909-1928 (2008).
7. Firoozjaee, A.R. and Afshar, M.H. "Discrete least square method (DLSM) for the solution of free surface seepage problem", *International Journal of Civil Engineerng*, **5**(2), pp. 134-143 (2007).
8. Firoozjaee, A.R. and Afshar, M.H. "Discrete least squares meshless method with sampling points for the solution of elliptic partial differential equations", *Engineering Analysis with Boundary Elements*, **33**(1), pp. 83-92 (2009).
9. Firoozjaee, A.R. and Afshar, M.H. "Steady-state solution of incompressible Navier-Stokes equations using discrete least-squares meshless method", *International Journal for Numerical Methods in Fluids*, **67**(3), pp. 369-382 (2010).
10. Shobeyri, G. and Afshar, M.H. "Efficient simulation of free surface flows with discrete least-squares meshless method using a priori error estimator", *International Journal of Computational Fluid Dynamics*, **24**(9), pp. 349-367 (2010).
11. Firoozjaee, A.R. and Afshar, M.H. "Error estimate and adaptive refinement for incompressible Navier-Stokes equations using the discrete least squares meshless method", *International Journal for Numerical Methods in Fluids*, **70**(1), pp. 56-70 (2012).
12. Zienkiewicz, O.C. and Taylor, R.L., *The Finite Element Method*, 5th Ed., Butterworth-Heinemann, Oxford, UK (2000).
13. Firoozjaee, A.R. and Afshar M.H. "Adaptive simulation of two dimensional hyperbolic problems by collocated discrete least squares meshless method", *Computers & Fluids*, **39**(10), pp. 2030-2039 (2010).
14. Chorin, A.J. "A numerical method for solving incompressible viscous flow problems", *Journal of Computational Physics*, **2**(1), pp. 12-26 (1967).
15. Goda, K. "A multistep technique with implicit difference schemes for calculating two- or three-dimensional cavity flows", *Journal of Computational Physics*, **30**(1), pp. 76-95 (1979).
16. Guermond, J.L., Minev, P. and Shen, J. "An overview of projection methods for incompressible flows", *Computer Methods in Applied Mechanics and Engineering*, **195**(44-47), pp. 6011-6045 (2006).
17. Guermond, J.L. and Quartapelle, L. "On stability and convergence of projection methods based on pressure Poisson equation", *International Journal for Numerical Methods in Fluids*, **26**(9), pp. 1039-1053 (1998).
18. Bell, B.C. and Surana, K.S. "P-version least squares finite element formulation for two dimensional, incompressible, non-Newtonian, isothermal and non-isothermal flow", *International. Journal of Numerical Methods in Fluids*, **18**, pp. 127-162 (1994).
19. Ghia, U.G. and Shin, C.T. "High-Re solutions for incompressible flow using the Navier-Stokes equations and a multigrid method", *Journal of Computational Physics*, **48**, pp. 387-411 (1982).

Biographies

Mohsen Lashckarbolok received his PhD degree in Water Engineering from Iran University of Science and Technology (IUST), Tehran, Iran. His research interests include error estimation and adaptive refinement techniques in Collocated Discrete Least Squares (CDLS) meshfree method and implementation of CDLS in solving non-Newtonian fluid flow.

Ebrahim Jabbari received his PhD degree in Hydraulic Engineering from the University of Leuven, Belgium, and is currently Associate Professor of Civil Engineering School at the Iran University of Science & Technology, Tehran, Iran. His research interests include numerical modeling of circulations in estuaries, numerical modeling of flow and sediment transport in rivers and coastal waters, and numerical analysis of non-Newtonian fluid flow.

Kees Vuik obtained his MS degree in Applied Mathematics from Delft University of Technology, the Netherlands, in 1982, and his PhD degree in Mathematics from Utrecht University, the Netherlands,in 1988. He is currently Professor in the Numerical Analysis Research Group at Delft University of Technology, Director of the Delft Center of Computational Science and Engineering, and Scientific Director of the 3TU.AMI, Applied Mathematics Institute.